Solution plasma assisted Mn-doping: A novel strategy for developing highly durable and active oxygen evolution catalysts

Hao He[a], Takeshi Matsuda[a], Akira Miura[b], Masanori Nagao[c], Jeevan Kumar Padarti[a], Tomoya Ohno[a], and Shigeto Hirai[*a]

[a] School of Earth, Energy and Environmental Engineering, Kitami Institute of Technology, 165 Koen-cho, Kitami 090-8507, Japan.

[b] Faculty of Engineering, Hokkaido University, Sapporo, Hokkaido, 060-8628, Japan.

[c] University of Yamanashi, 7-32 Miyamae, Kofu, Yamanashi 400-0021, Japan.

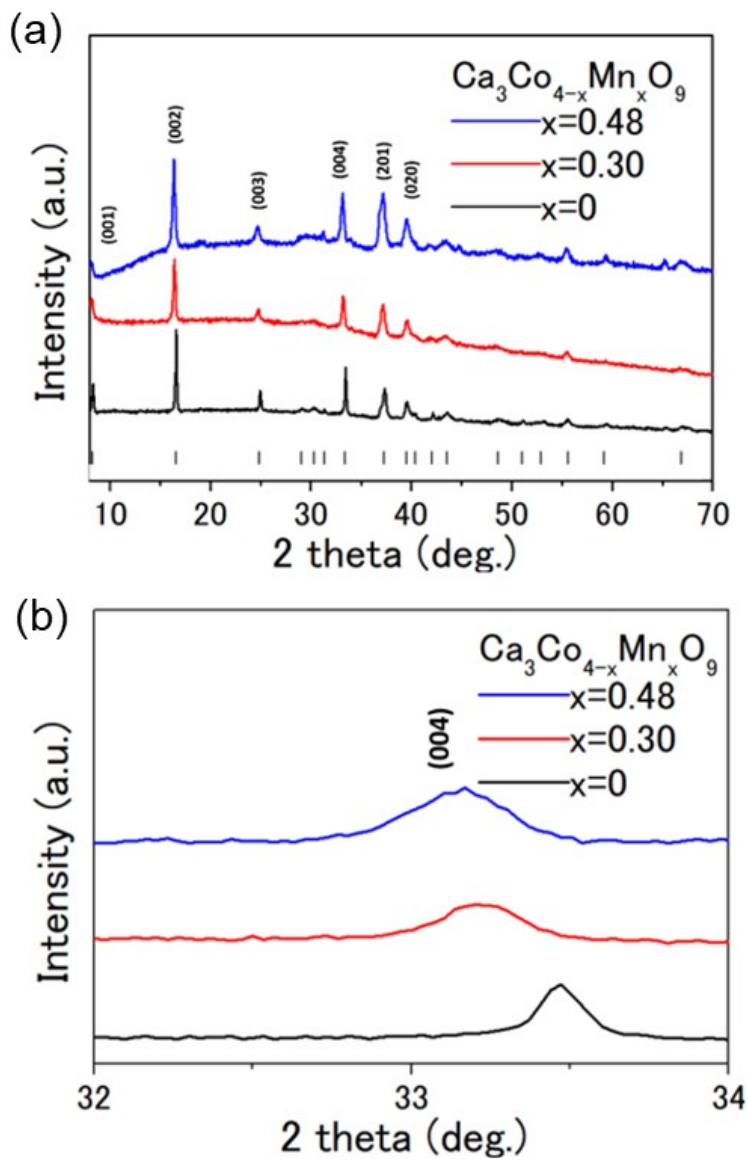* Corresponding author: e-mail hirai@mail.kitami-it.ac.jp

Supporting Information

Fig. S1. (a) X-ray diffraction profiles of $Ca_3Co_{4-x}Mn_xO_9$ (x=0,0.30,0.48) along with the Bragg position of $Ca_3Co_4O_9$. (b) Expanded view of the (0 0 4) peak for $Ca_3Co_{4-x}Mn_xO_9$.
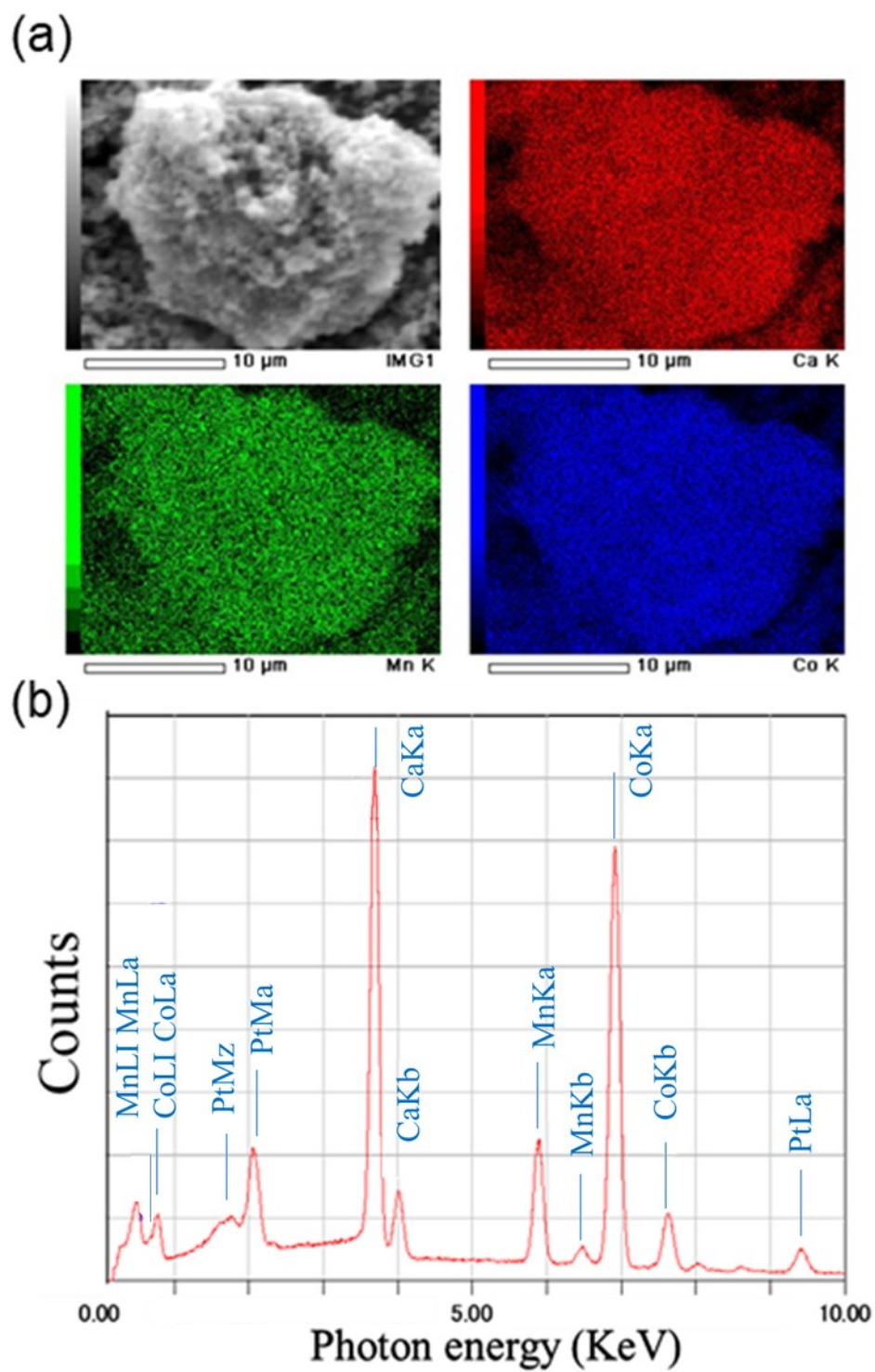
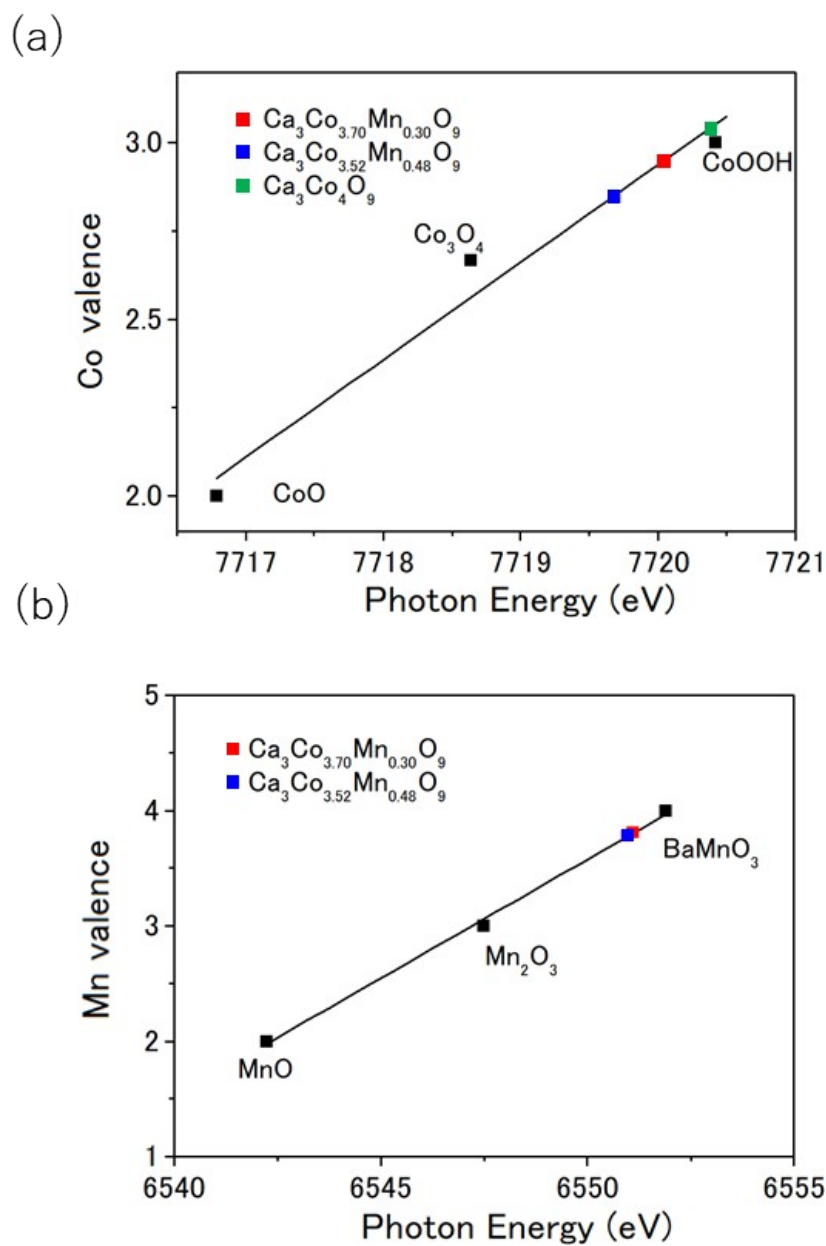**Fig. S2.** SEM image of $Ca_3Co_{4-x}Mn_xO_9$. The representative SEM image, EDX elemental mapping, and EDX spectrum of $Ca_3Co_{4-x}Mn_xO_9$ (x=0.48).

**Fig. S3.** Co and Mn K-edge X-ray absorption near-edge structure (XANES) spectra for $Ca_3Co_{4-x}Mn_xO_9$ (x=0,0.30,0.48). (a) Co valence of pristine $Ca_3Co_{4-x}Mn_xO_9$ (x=0, 0.30,0.48), CoO, Co_3O_4, and CoOOH as a function of the photon energy for the Co K-edge peak. Therefore, the average Co valence is between 2.67 and 3. (b) Mn valence of pristine $Ca_3Co_{4-x}Mn_xO_9$ (x=0, 0.30,0.48), MnO, Mn_2O_3, and $BaMnO_3$ as a function of the photon energy for the Mn K-edge peak. Therefore, the average Mn valence is between 3 and 4.
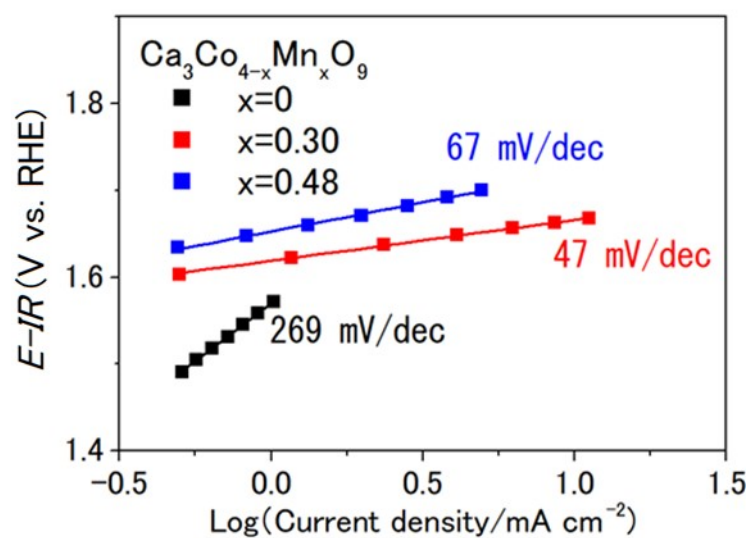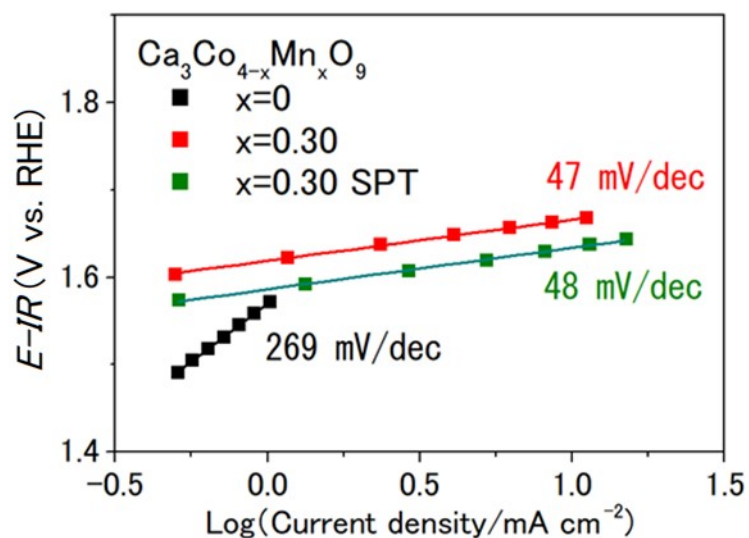
Fig. S4. Tafel plots of $Ca_3Co_{4-x}Mn_xO_9$. (a) Tafel plots for $Ca_3Co_4O_9$, $Ca_3Co_{3.70}Mn_{0.30}O_9$, and $Ca_3Co_{3.52}Mn_{0.48}O_9$. (b) Tafel plots for $Ca_3Co_4O_9$, $Ca_3Co_{3.70}Mn_{0.30}O_9$, and $Ca_3Co_{3.70}Mn_{0.30}O_9$ after the solution plasma treatment.
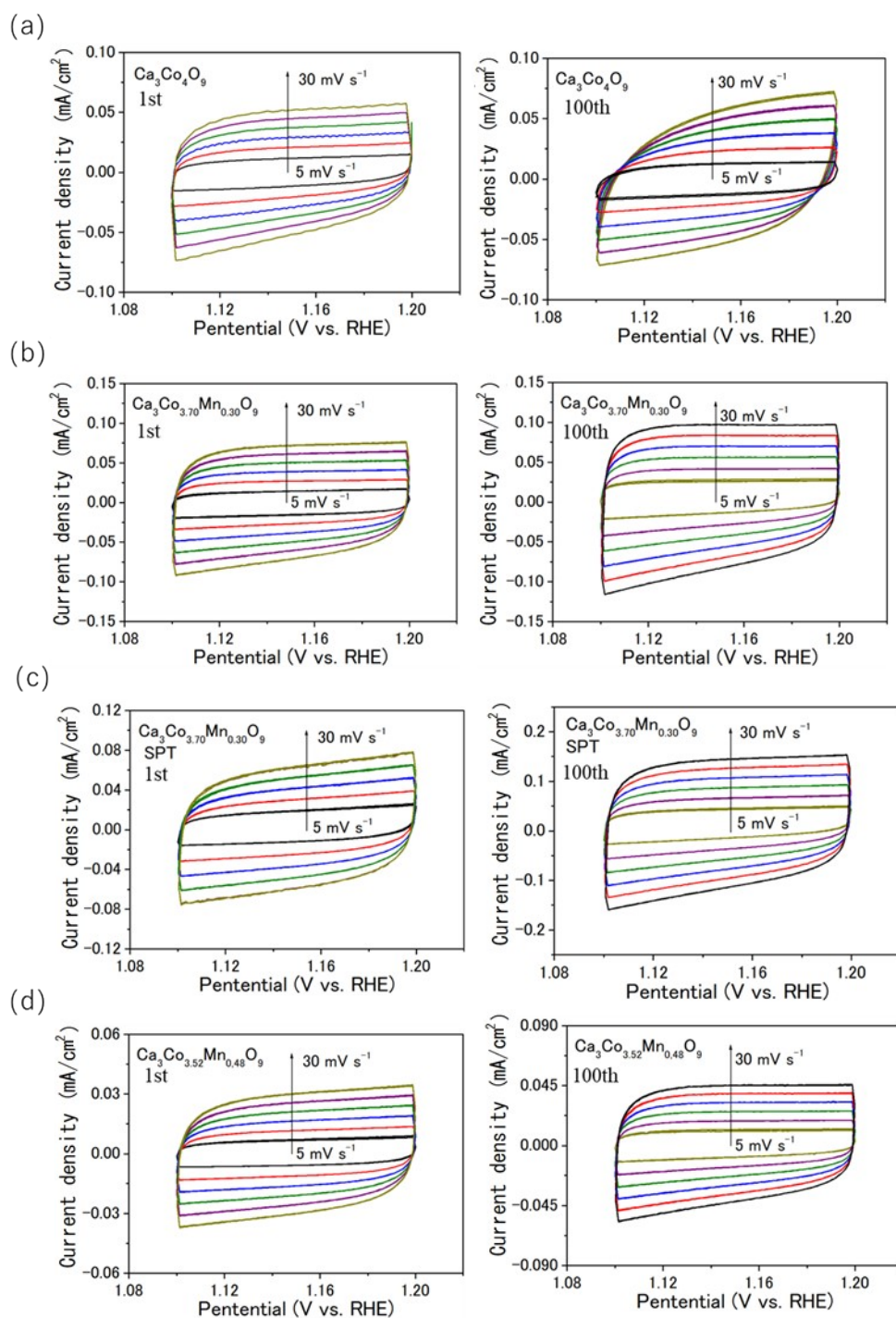
Fig. S5. Calculation of the double layer capacitance for $Ca_3Co_{4-x}Mn_xO_9$(x=0, 0.30, 0.48, 0.30 SPT) at the 1st and 100th OER cycle. The cyclic voltammograms measured from 0.174−0.274 V vs. Hg/HgO in 0.1 M KOH aqueous solution at the scan rate of 10 mV/s.
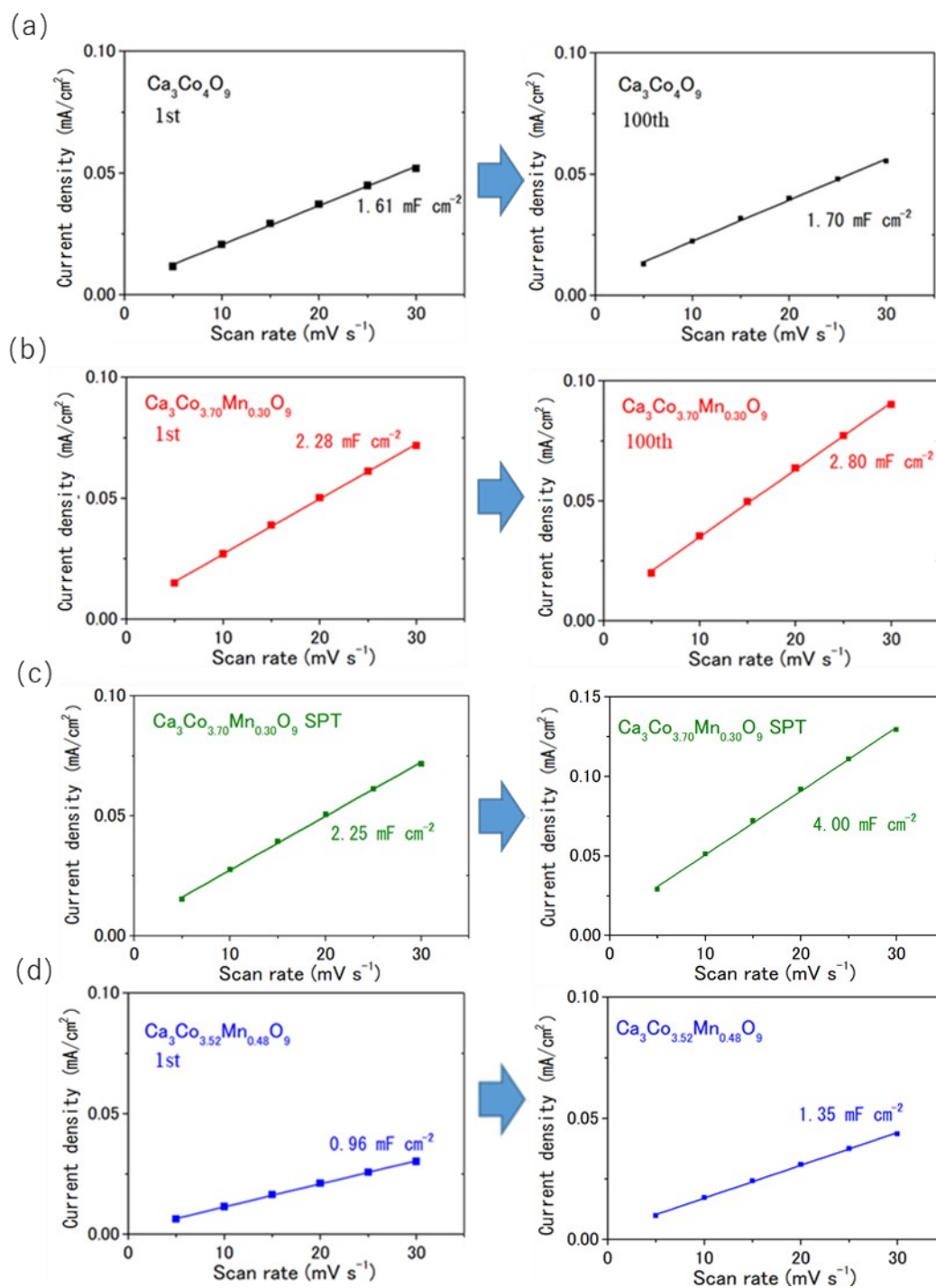
Fig. S6. The scan rate dependence of the current density at 1.15 V vs. RHE in 0.1 M KOH aqueous solution at the scan rate of 10 mV/s for $Ca_3Co_{4-x}Mn_xO_9$(x=0, 0.30, 0.48, 0.30 SPT) at the 1st and 100th OER cycle.

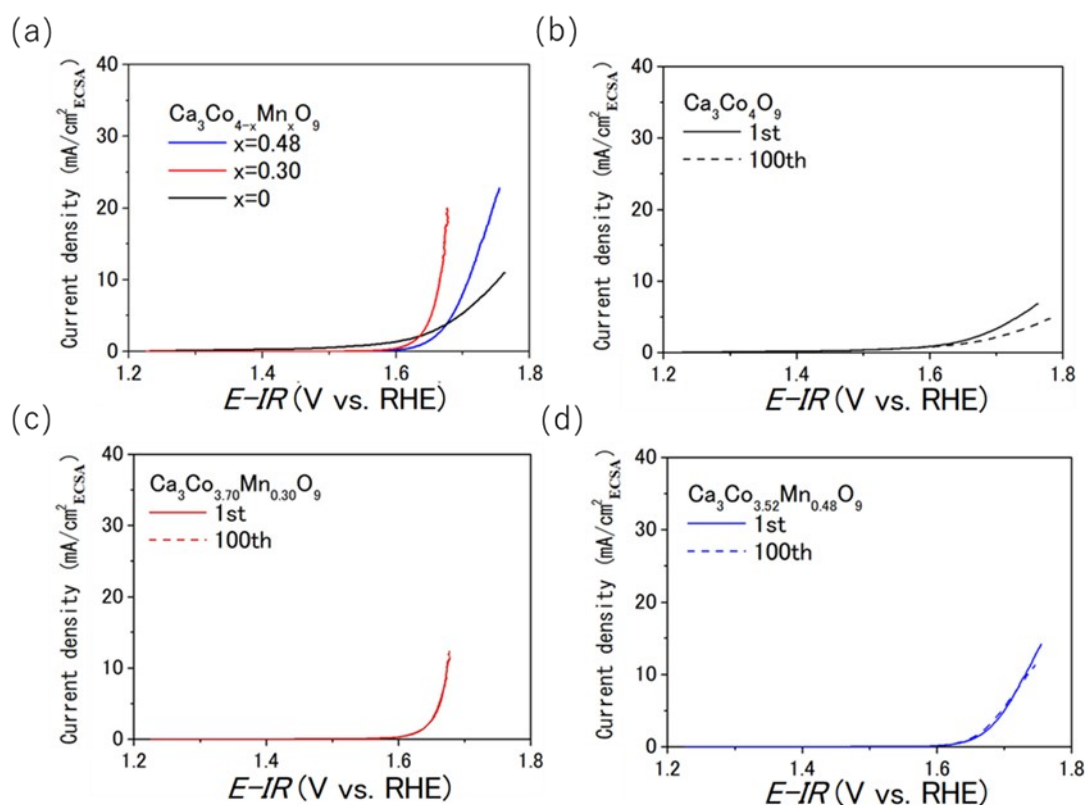**Fig. S7.** The OER activity of $Ca_3Co_{4-x}Mn_xO_9$(x=0,0.30,0.48). (a) The linear sweep voltammograms for $Ca_3Co_{4-x}Mn_xO_9$(x=0,0.30,0.48) in 0.1 M KOH aqueous solution normalized to the relative ECSA determined from the slope of Fig. S6. Linear sweep voltammograms at the 1st and 100th cycle for (b) $Ca_3Co_4O_9$, (c) $Ca_3Co_{4-x}Mn_xO_9$ (x=0.30), and (d) $Ca_3Co_{4-x}Mn_xO_9$ (x=0.48) in 0.1 M KOH aqueous solution normalized to the relative ECSA determined from the slope of Fig. S6.

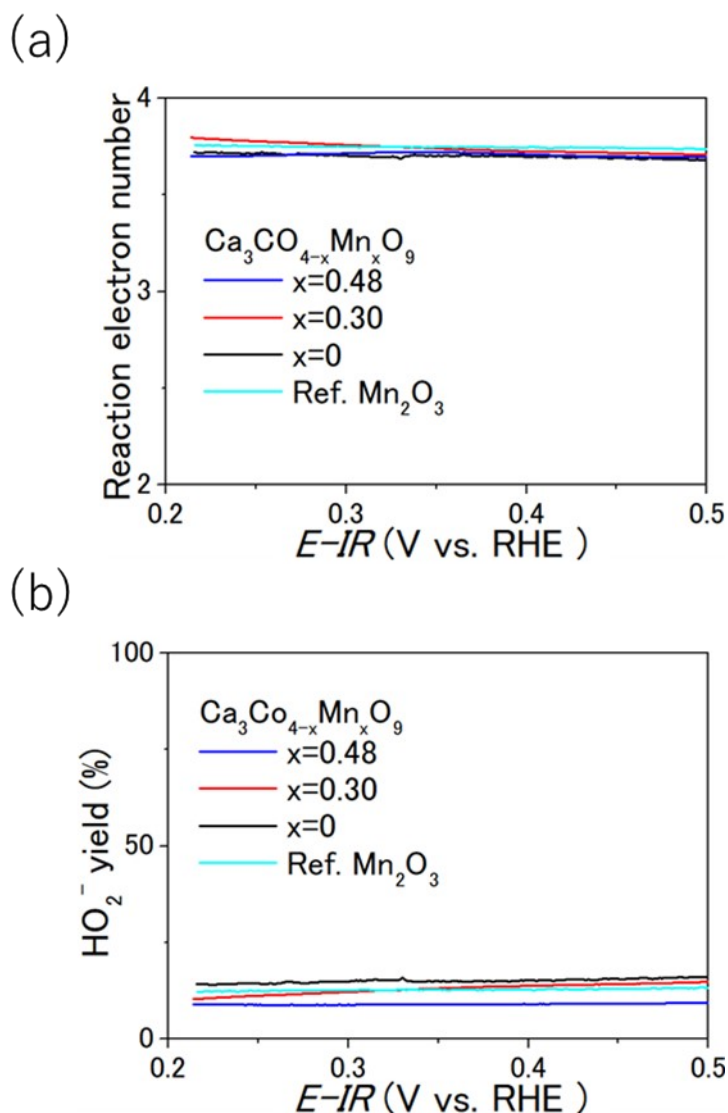**Fig. S8.** (a) The reaction electron number of the ORR for $Ca_3Co_{4-x}Mn_xO_9$ (x=0, 0.30, 0.48) in 0.1 M KOH aqueous solution at the scan rate of 10 mV/s. Mn_2O_3 nanoparticle is shown as a standard of a highly active ORR catalyst. The reaction electron numbers (ne)were calculated using $\dfrac{4NI_d}{NI_d + I_r}$, where I_d is the disk current density, I_r is the ring current density, and N (=0.42) is the current collection efficiency. (b) The hydrogen peroxide yield of the ORR for $Ca_3Co_{4-x}Mn_xO_9$ (x=0, 0.30, 0.48) before and after the solution plasma treatment measured in 0.1 M KOH aqueous solution at the scan rate of 10 mV/s. The hydrogen peroxide yield was calculated using HO_2^- (%) $= \dfrac{200I_r}{NI_d + I_r}$.
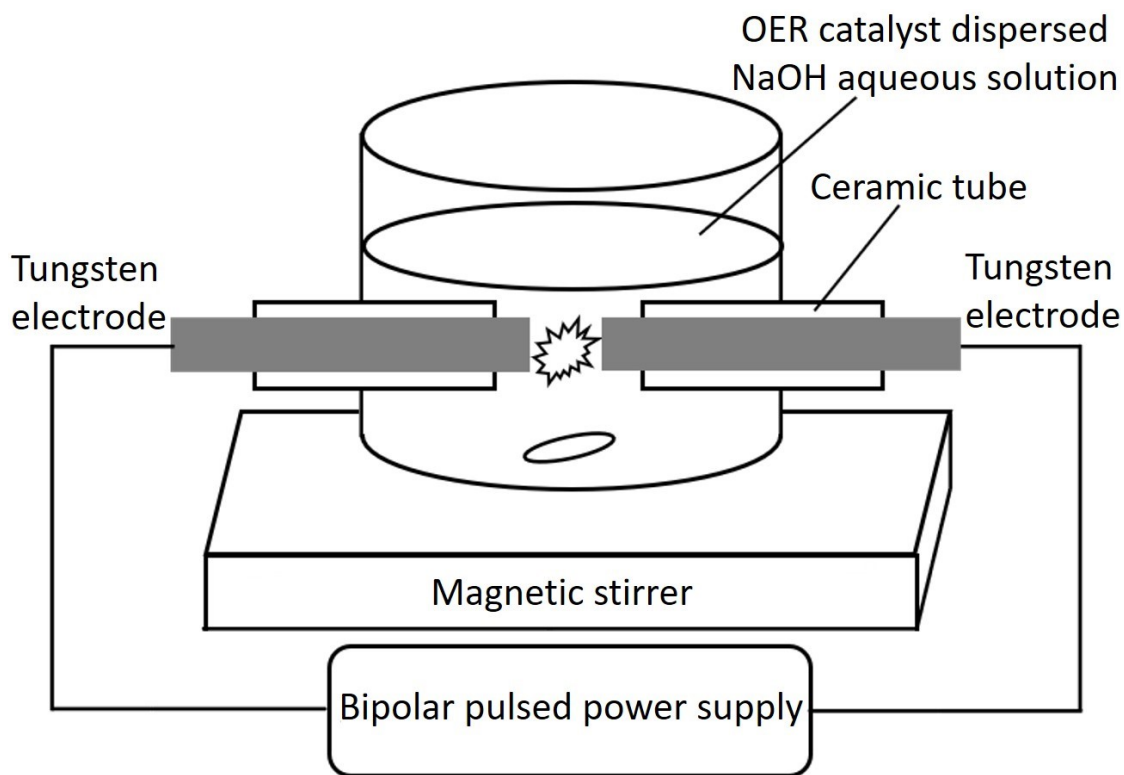
Fig. S9. Schematic image of the system used for the solution plasma treatment of the OER catalyst. In the present study, the solution plasma treatment of $Ca_3Co_{4-x}Mn_xO_9$ (x=0.30) was conducted in 0.01 M NaOH aqueous solution.

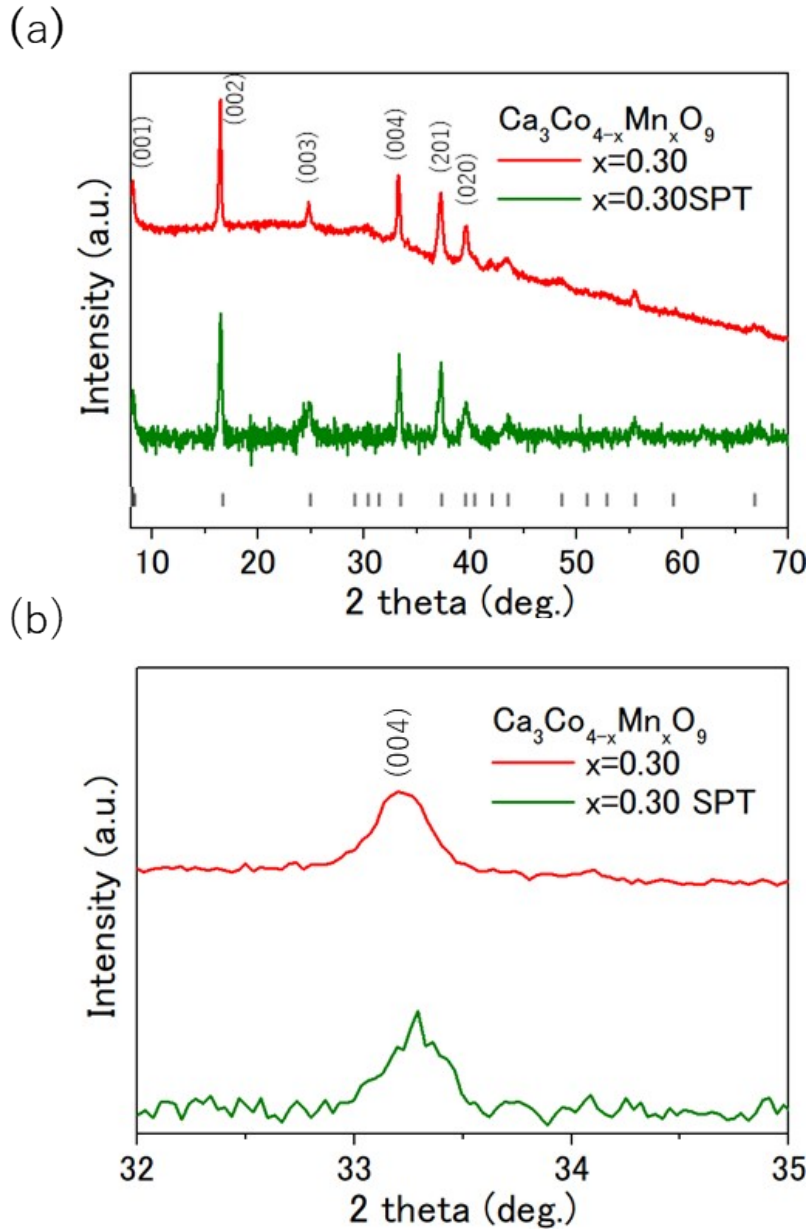**Fig. S10.** (a) X-ray diffraction profiles and (b) the expanded view of the (0 0 4) peak for $Ca_3Co_{4-x}Mn_xO_9$ (x=0.3) before and after the solution plasma treatment. $Ca_3Co_{4-x}Mn_xO_9$ after the solution plasma treatment is denoted as SPT.

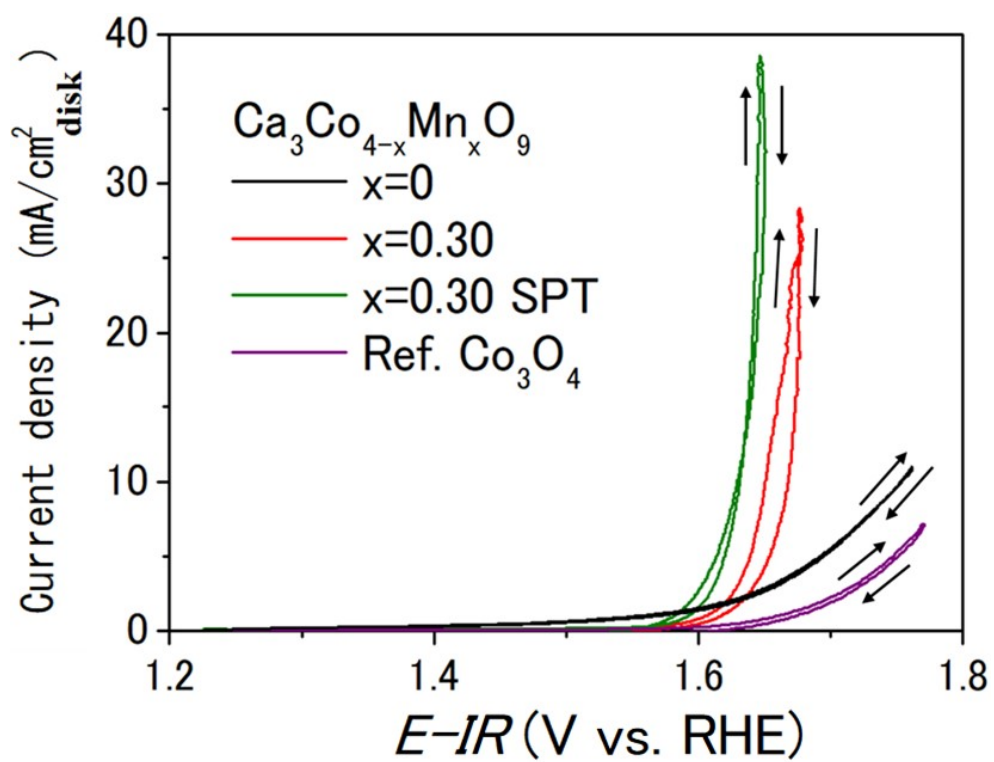**Fig. S11.** The cyclic voltammograms of $Ca_3Co_{4-x}Mn_xO_9$ (x=0,0.30,0.30 SPT) for OER in 0.1 M KOH aqueous solution normalized to the disk electrode area. $Ca_3Co_{4-x}Mn_xO_9$ after the solution plasma treatment is denoted as SPT.

(a)

(b)

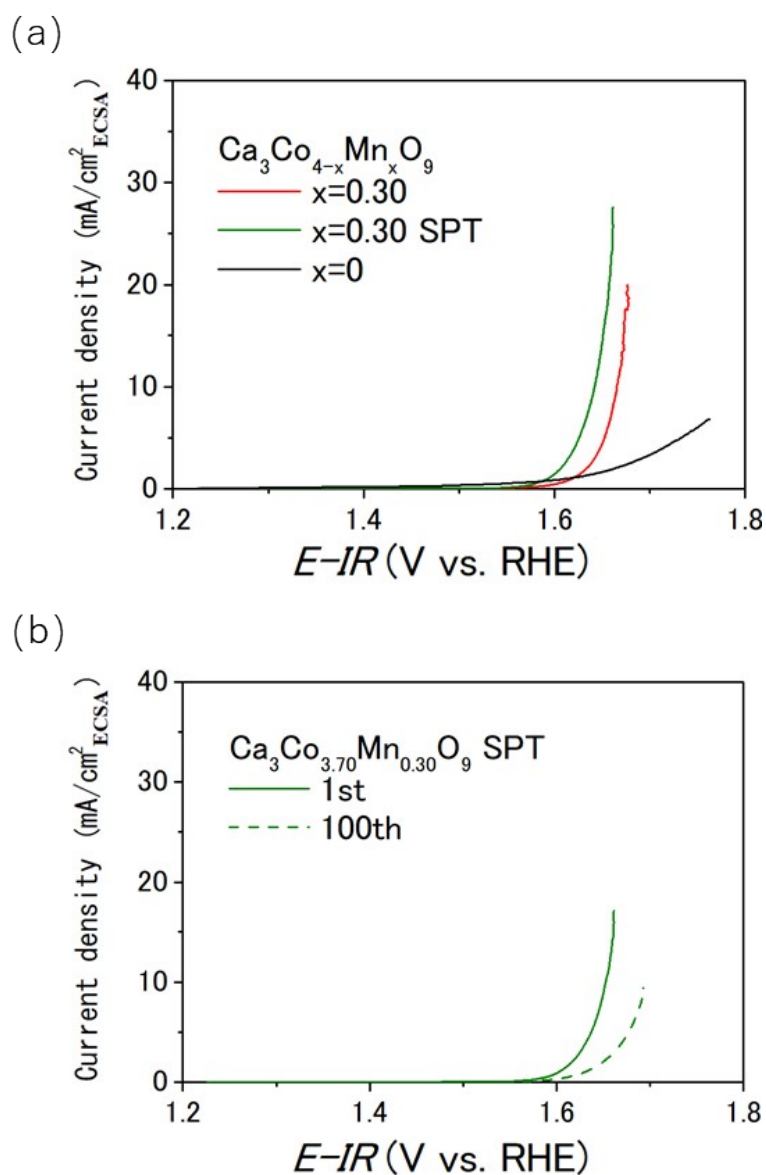**Fig. S12.** (a) Linear sweep voltammograms of $Ca_3Co_{4-x}Mn_xO_9$ (x=0,0.30,0.30 SPT) for OER in 0.1 M KOH aqueous solution normalized to the relative ECSA determined from the slope of Fig. S6. (b) Linear sweep voltammograms of the 1st and 100th cycle for $Ca_3Co_{3.70}Mn_{0.30}O_9$ in 0.1 M KOH aqueous solution normalized to the relative ECSA determined from the slope of Fig. S6.

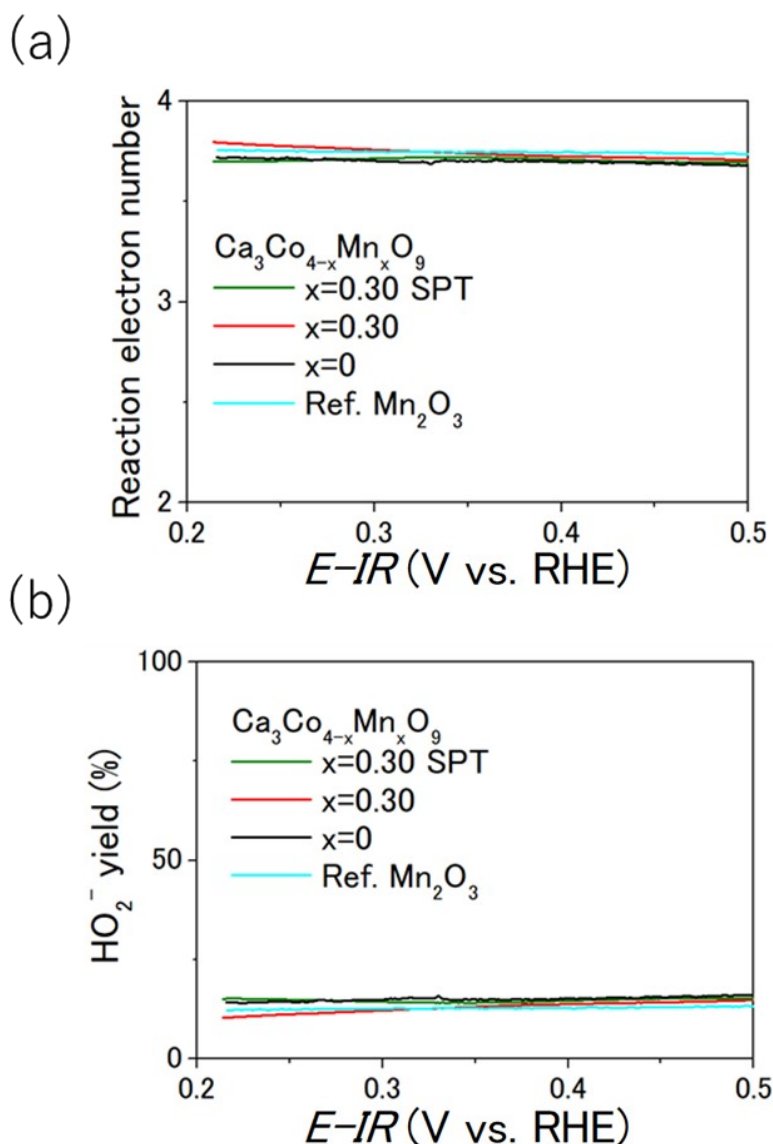**Fig. S13.** (a)The reaction electron number of the ORR for $Ca_3Co_{4-x}Mn_xO_9$ (x=0.3) before and after the solution plasma treatment measured in 0.1 M KOH aqueous solution. Mn_2O_3 nanoparticle is shown as a standard of a highly active ORR catalyst. The reaction electron numbers (ne)were calculated using $\dfrac{4NI_d}{NI_d + I_r}$, where I_d is the disk current density, I_r is the ring current density, and N (=0.42) is the current collection efficiency. (b) The hydrogen peroxide yield of the ORR for $Ca_3Co_{4-x}Mn_xO_9$ (x=0.3) before and after the solution plasma treatment measured in 0.1 M KOH aqueous solution. The hydrogen peroxide yield for $Ca_3Co_4O_9$ is shown as a reference. The hydrogen peroxide yield was calculated using
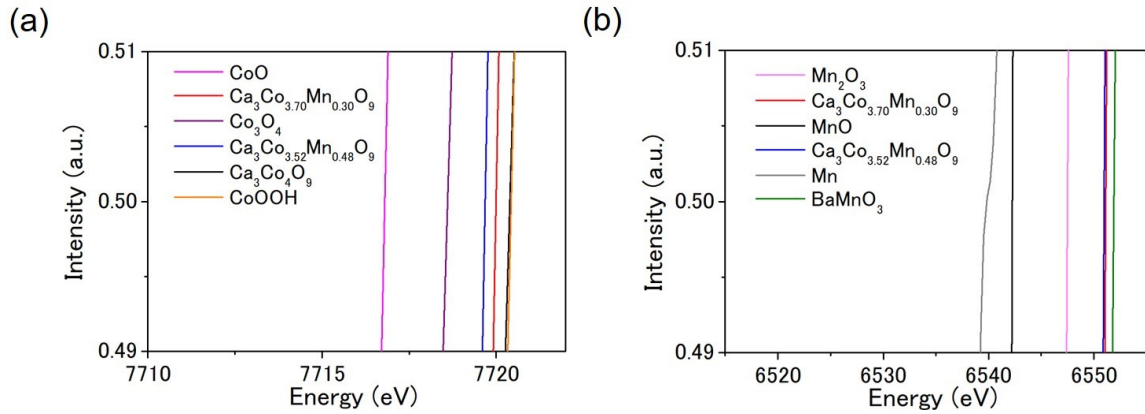
$$HO_2^- (\%) = \frac{200I_r}{NI_d + I_r}.$$

(a)

(b)

Fig. S14. (a) Expanded view of the Co K-edge X-ray absorption near-edge structure (XANES) spectra for $Ca_3Co_{4-x}Mn_xO_9$ (x=0, 0.30, 0.48). Co K-edge XANES spectra of CoO, Co_3O_4, and CoOOH were collected as standard materials. (b) Expanded view of the Mn K-edge X-ray absorption near-edge structure (XANES) spectra for $Ca_3Co_{4-x}Mn_xO_9$ (x=0, 0.30, 0.48). Mn K-edge XANES spectra of MnO, Mn_2O_3, and $BaMnO_3$ were collected as standard materials.

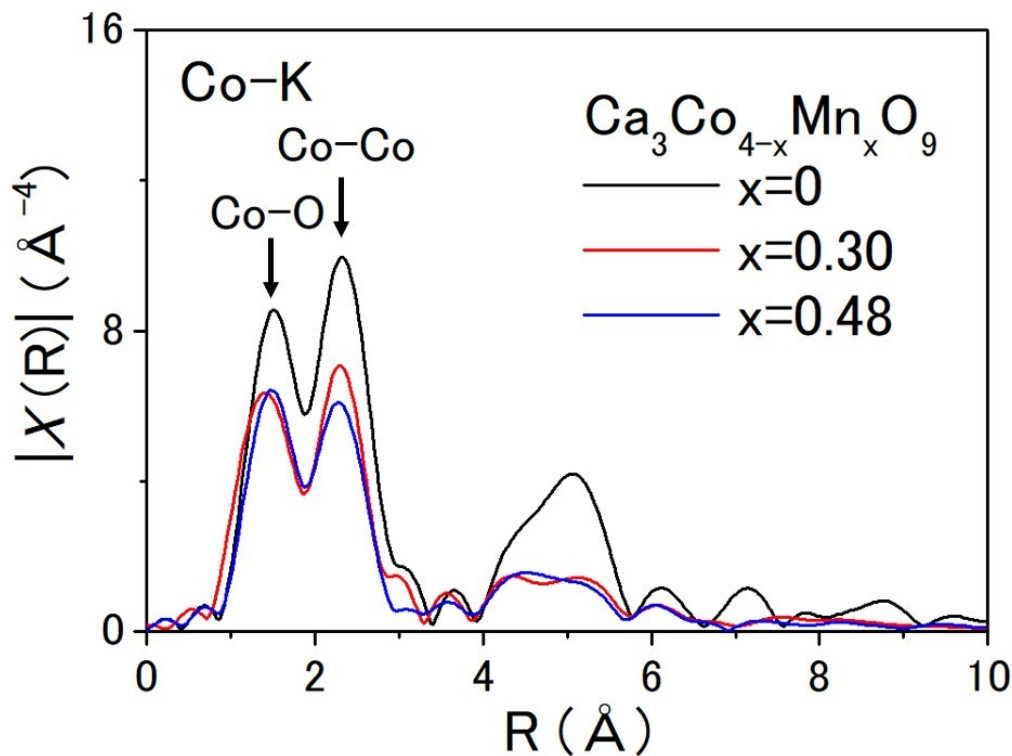**Fig. S15.** Fourier transformed k^3-weighted Co K-edge EXAFS for $Ca_3Co_{4-x}Mn_xO_9$ (x=0,

0.30, 0.48) in the representation form of $|X(\text{R})|$.
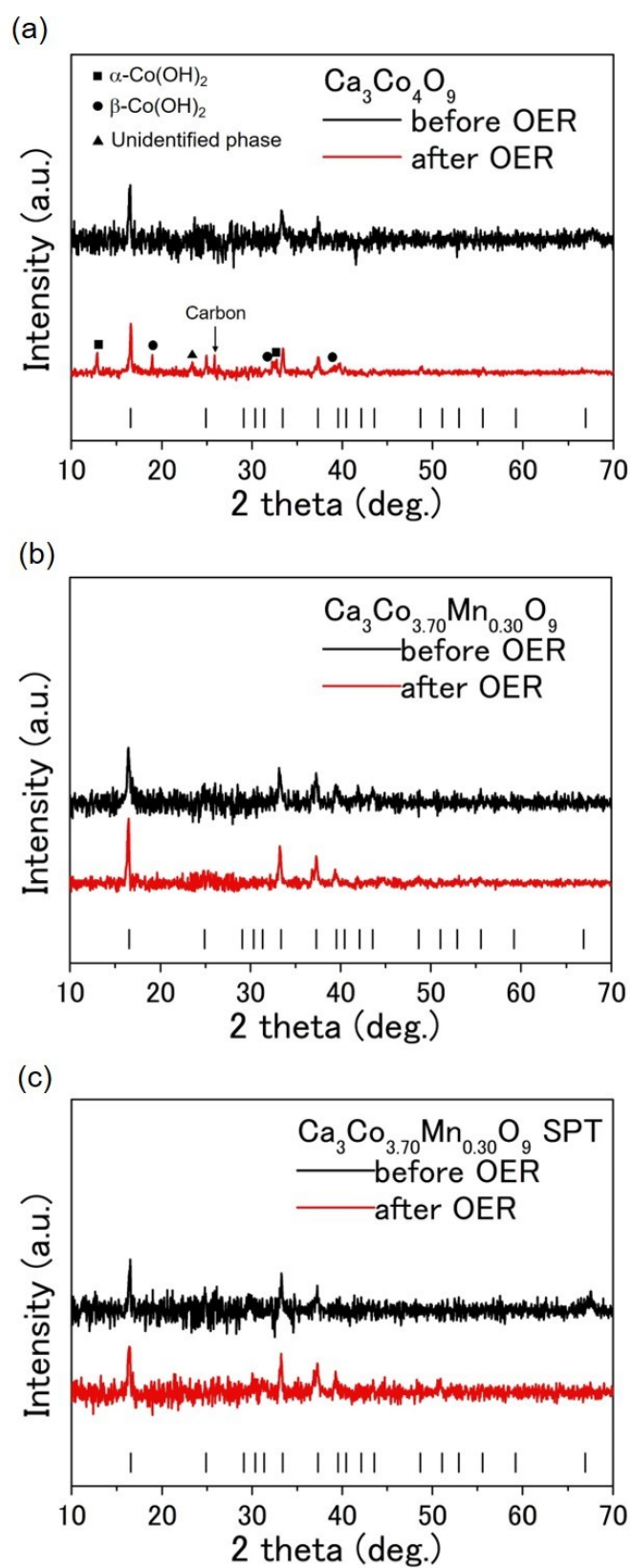
Fig. S16. X-ray diffraction profiles of $Ca_3Co_4O_9$, $Ca_3Co_{4-x}Mn_xO_9$ (x=0.30), and $Ca_3Co_{4-x}Mn_xO_9$ (x=0.30 SPT) before and after the OER cycle stability test, along with the Bragg

position of $Ca_3Co_4O_9$. For $Ca_3Co_4O_9$, new diffraction peaks of α-$Co(OH)_2$ (JCPDS #46-0605) and β-$Co(OH)_2$ (JCPDS #45-0036) were detectable after the OER test, suggesting the surface decomposition during the OER. The unidentified phase (its diffraction peak is denoted as triangle) is likely to be the product of the surface decomposition of $Ca_3Co_4O_9$.

(a) $Ca_3Co_{4-x}Mn_xO_9$ (x=0.30)
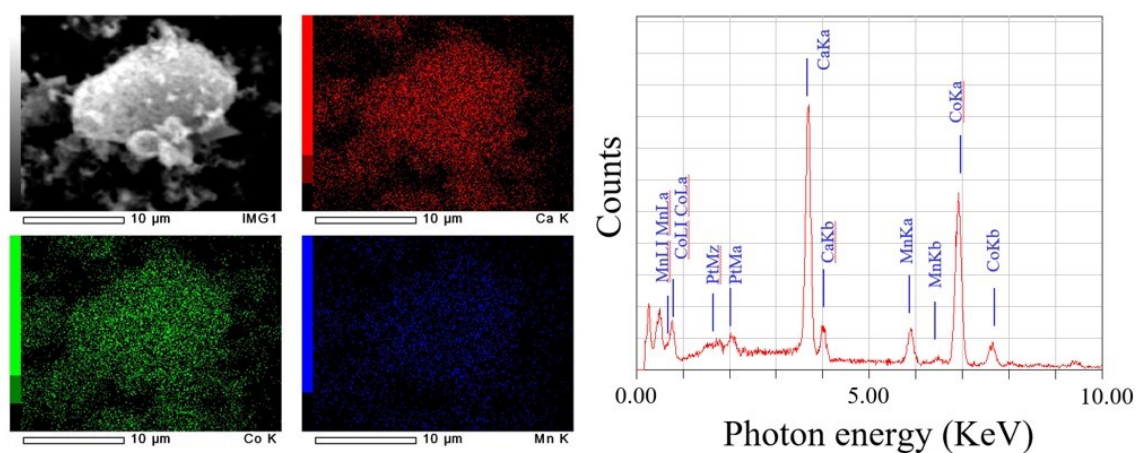
(b) $Ca_3Co_{4-x}Mn_xO_9$ (x=0.30 SPT)
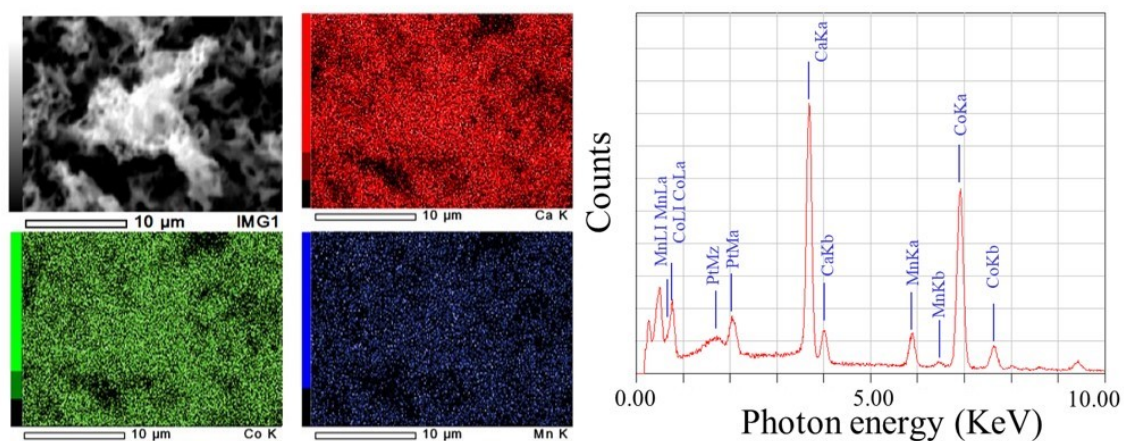
Fig. S17. SEM images, EDX elemental mapping, and EDX spectra of $Ca_3Co_{4-x}Mn_xO_9$ (x=0.30) before and after the solution plasma treatment. $Ca_3Co_{4-x}Mn_xO_9$ (x=0.30) after the solution plasma treatment is denoted as SPT.
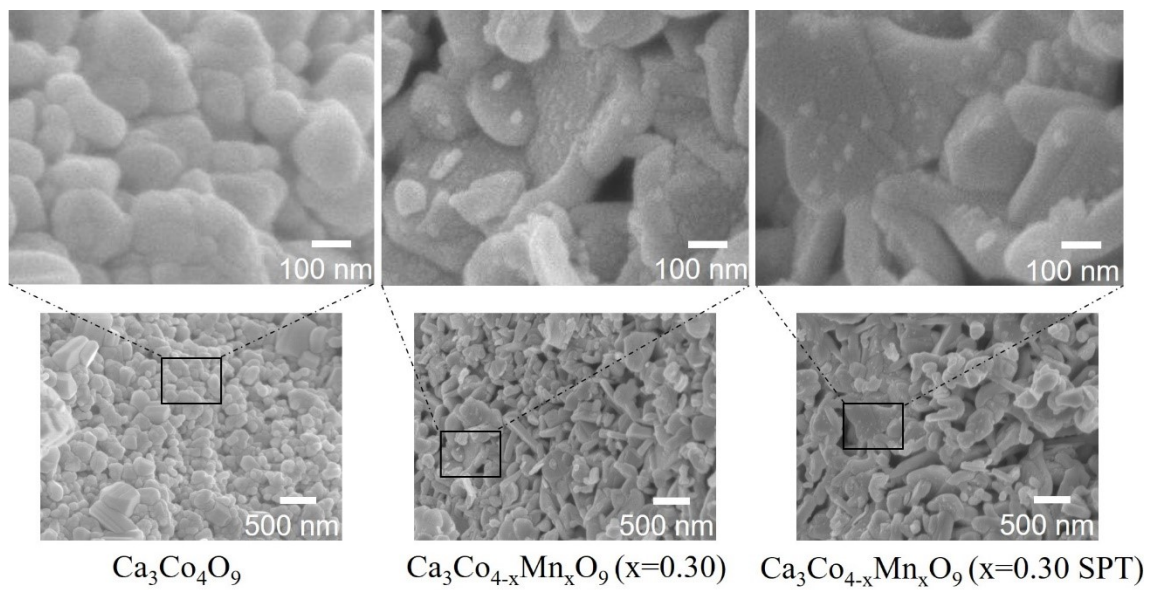
Fig. S18. FE-SEM images of $Ca_3Co_{4-x}Mn_xO_9$ (x=0,0.30,0.30 SPT) along with the magnified images. $Ca_3Co_{4-x}Mn_xO_9$ (x=0.30) after the solution plasma treatment is denoted as SPT.
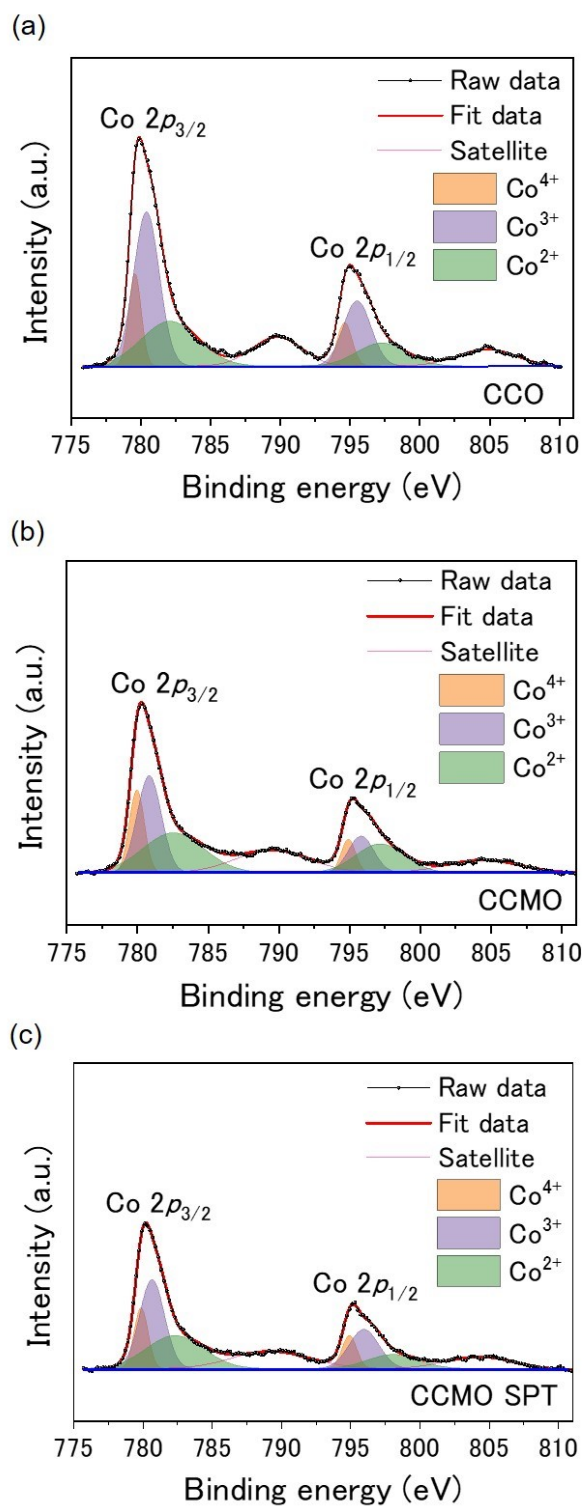
Fig. S19. Co $2p$ core-level spectra for (a) $Ca_3Co_4O_9$, (b) $Ca_3Co_{4-x}Mn_xO_9$ (x=0.30), and (c) $Ca_3Co_{4-x}Mn_xO_9$ (x=0.30 SPT).
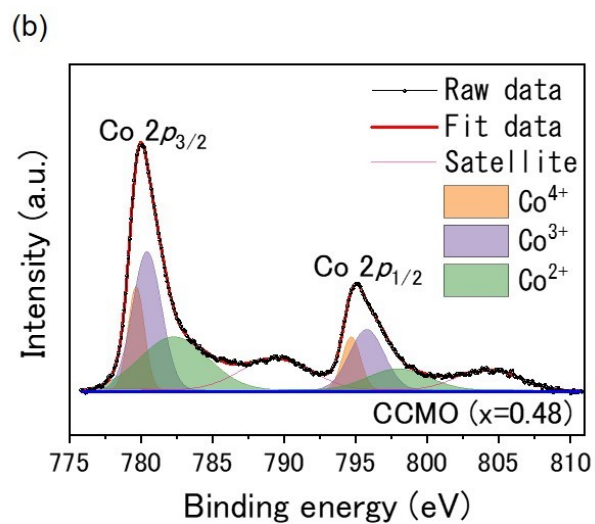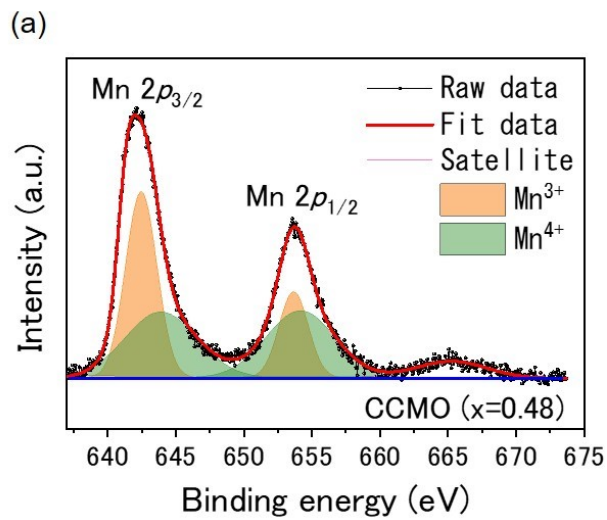
Fig. S20. (a) Mn $2p$ core-level spectra for $Ca_3Co_{4-x}Mn_xO_9$ (x=0.48). (b) Co $2p$ core-level spectra for $Ca_3Co_{4-x}Mn_xO_9$ (x=0.48).

(a) $Ca_3Co_4O_9$ after OER
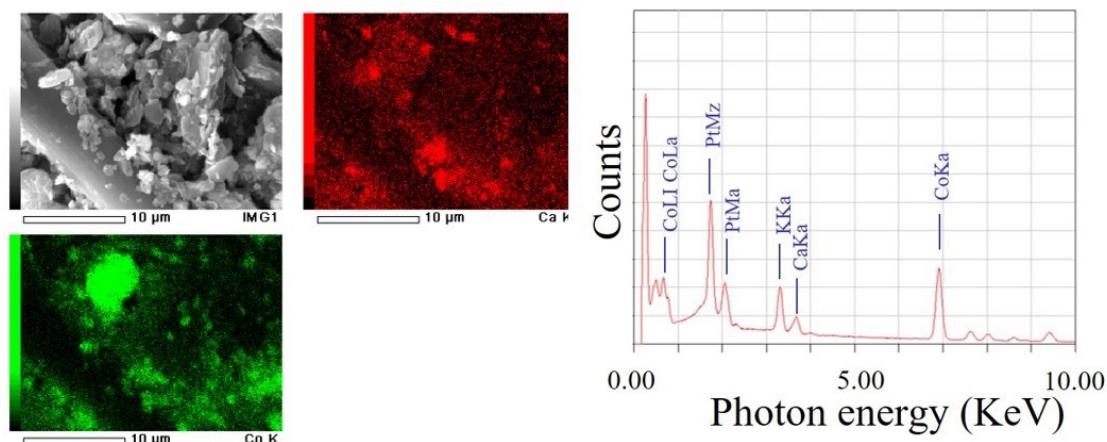
(b) $Ca_3Co_{4-x}Mn_xO_9$ (x=0.30) after OER
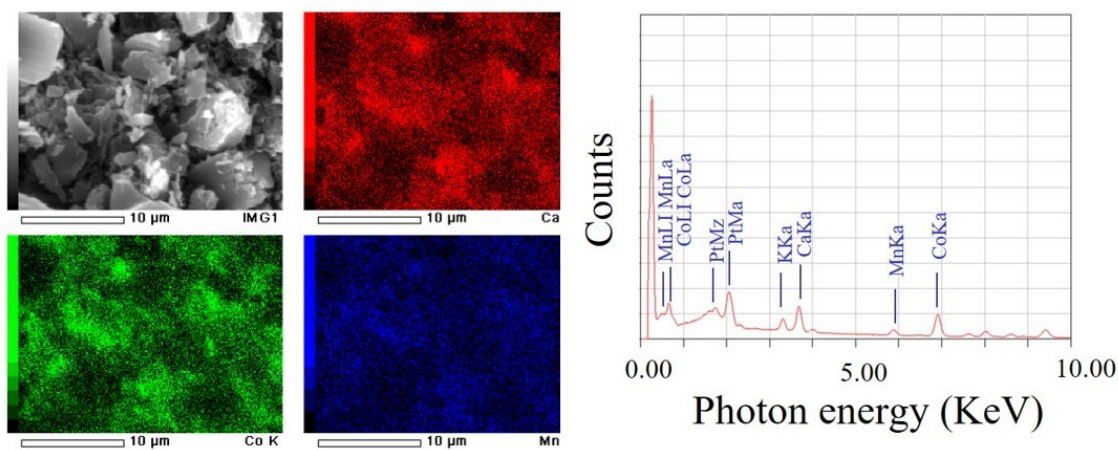
(c) $Ca_3Co_{4-x}Mn_xO_9$ (x=0.30 SPT) after OER
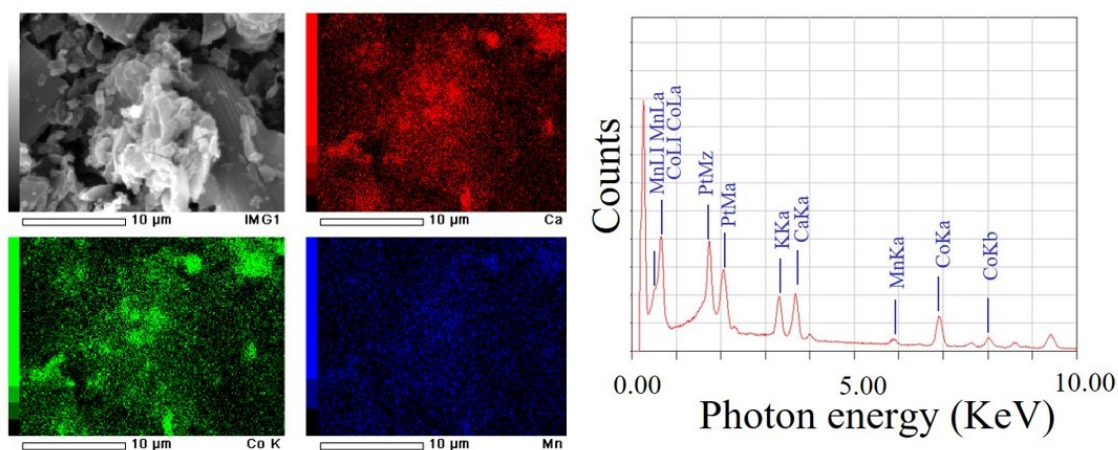
Fig. S21. SEM images, EDX elemental mapping, and EDX spectra of $Ca_3Co_4O_9$, $Ca_3Co_{4-x}Mn_xO_9$ (x=0.30), and $Ca_3Co_{4-x}Mn_xO_9$ (x=0.30 SPT) after the OER cycle stability test. Carbon paper, acetylene black, and Nafion from the OER test is present in the SEM

image.
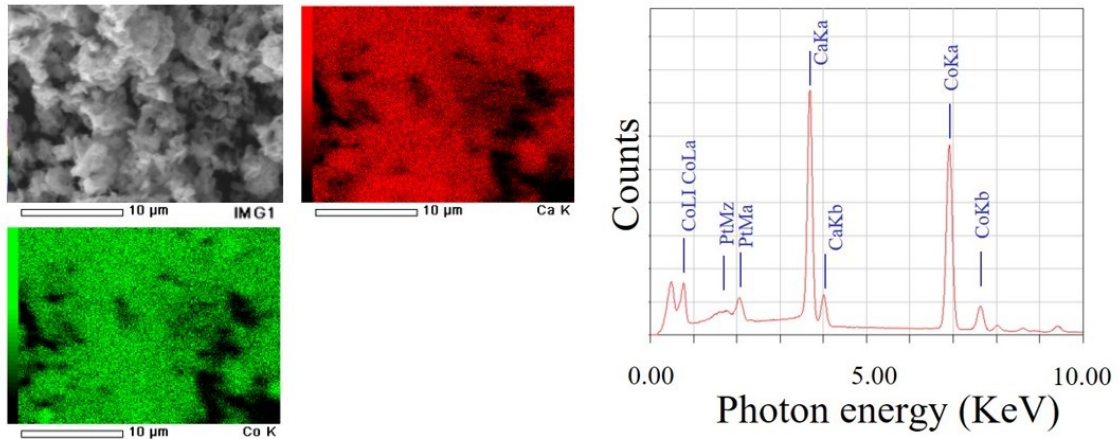
Fig. S22. SEM image, EDX elemental mapping, and EDX spectrum of $Ca_3Co_4O_9$ before the OER cycle stability test.
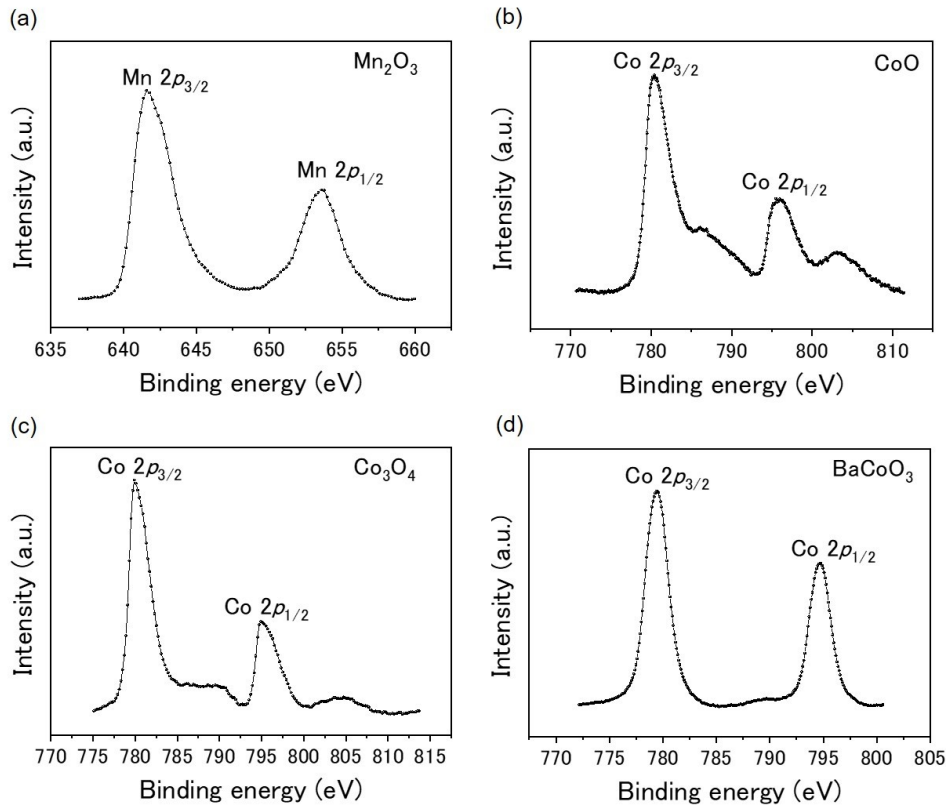
Fig. S23. Mn and Co $2p$ core-level spectra of the reference samples. (a) Mn $2p$ core-level spectra of Mn_2O_3 (Mn $2p_{3/2}$ peak: 641.7 eV and Mn $2p_{1/2}$ peak: 653.5 eV). (b) Co $2p$ core-level spectra of CoO (Co $2p_{3/2}$ peak: 780.4 eV and Co $2p_{1/2}$ peak: 796.0 eV). (c) Co $2p$ core-level spectra of Co_3O_4 (Co $2p_{3/2}$ peak: 779.8 eV and Co $2p_{1/2}$ peak: 794.9 eV). (d) Co $2p$ core-level spectra of $BaCoO_3$ (Co $2p_{3/2}$ peak: 779.4 eV and Co $2p_{1/2}$ peak: 794.7

eV).

Table S1. OER performance for $Ca_3Co_{4-x}Mn_xO_9$ (x=0, 0.30, 0.48, 0.30 SPT) in 0.1 M KOH aqueous solution. Co_3O_4 nanoparticle is shown as a standard of a highly active OER catalyst. The overpotential (η) at 0.5 mA/cm² was determined from the onset potential (E_{onset}) by $\eta = E_{onset} - 1.23$ V. The turnover frequency (TOF) was calculated by TOF = $j/4Fn$, where j is the OER current at 1.66 V vs. RHE, F is the Faraday constant, and n is the number of moles of the Co atom on the working electrode.

Materials	Current density (mA/cm²) 1st @ 1.66 V vs. RHE	Current density (mA/cm²) 100th @ 1.66 V vs. RHE
Co_3O_4	1.00	2.83
CCO	3.06	2.31
CCMO(x=0.30)	10.76	11.84
CCMO(x=0.48)	1.32	2.22
CCMO(x=0.30) SPT	32.47	11.55

Materials	Overpotential η (V) 1st	overpotential η (V) 100th
Co_3O_4	0.40	0.37
CCO	0.10	0.26
CCMO(x=0.30)	0.37	0.39
CCMO(x=0.48)	0.40	0.39
CCMO(x=0.30) SPT	0.34	0.35

Materials	TOF (s⁻¹) 1st	TOF (s⁻¹) 100th
Co_3O_4	8.18×10^{-4}	2.31×10^{-3}
CCO	3.89×10^{-3}	2.94×10^{-3}
CCMO(x=0.30)	1.48×10^{-2}	1.62×10^{-2}
CCMO(x=0.48)	1.90×10^{-3}	3.20×10^{-3}

CCMO(x=0.30) SPT	$4..45\times10^{-2}$	1.58×10^{-2}

Table S2. The resistance elements of the equivalent circuit for $Ca_3Co_4O_9$ and the Mn-doped $Ca_3Co_{3.70}Mn_{0.30}O_9$. These results were obtained by fitting the electrochemical impedance spectra (EIS) of $Ca_3Co_4O_9$ and $Ca_3Co_{3.70}Mn_{0.30}O_9$ with the equivalent circuit in Fig. 3g at 0.7 V vs. Hg/HgO. R_s, R_t, and R_{ct} denote the solution resistance, film resistance, charge transfer resistance.

	CCO	CCMO(x=0.30)	CCMO(x=0.30) SPT
R_s（Ω）	43	43	43
R_t（Ω）	80	80	80
R_{ct}（Ω）	450	292	16

Table S3. ORR performance for $Ca_3Co_{4-x}Mn_xO_9$ (x=0, 0.30, 0.48, 0.30 SPT) in 0.1 M KOH aqueous solution. Mn_2O_3 and Pt/C (20 wt.% load, Sigma-Aldrich) are shown as standards of highly active ORR catalysts. The overpotential (η) at 0.5 mA/cm^2 was determined from the onset potential (E_{onset}) by $\eta = 1.23$ V $- E_{onset}$.

Materials	Current density (mA/cm^2) @ 0.30 V vs. RHE	Overpotential η (V)
Mn_2O_3	2.39	0.50
Pt/C	4.10	0.38
CCO	1.38	0.66
CCMO(x=0.30)	1.52	0.51
CCMO(x=0.48)	1.28	0.62
CCMO(x=0.30) SPT	1.56	0.54

Table S4. Mn/Co ratio of $Ca_3Co_{4-x}Mn_xO_9$ (x=0.30) before and after the solution plasma treatment. The Mn/Co ratio of $Ca_3Co_{4-x}Mn_xO_9$ (x=0.48) is also shown. The Mn/Co ratio was determined by X-ray photoemission spectroscopy (XPS). Integrated peak areas of the Mn and Co $2p$ core-level spectra (Fig. 6, Fig. S19, and Fig. S20) were used for calculating the Mn/Co ratio. The Mn/Co ratio determined by the Mn content x that follows the Vegard's law (Fig. 1b) is shown for comparison. Furthermore, we show the Mn/Co ratio determined by the SEM/EDX analysis (Fig. S2, Fig. S17, Fig. S21, and Fig. S22).

Materials	Mn/Co ratio from XPS	Mn/Co ratio from Vegard's law	Mn/Co ratio from EDX
CCMO(x=0.30)	0.38	0.08	0.15
CCMO(x=0.30) SPT	0.32	0.08	0.14
CCMO(x=0.48)	0.31	0.14	0.19

Table S5. Mn^{3+}/Mn^{4+} ratio of $Ca_3Co_{4-x}Mn_xO_9$ (x=0.30) before and after the solution plasma treatment. The Mn^{3+}/Mn^{4+} ratio of $Ca_3Co_{4-x}Mn_xO_9$ (x=0.48) is also shown. The Mn^{3+}/Mn^{4+} ratio was determined by X-ray photoemission spectroscopy (XPS). Integrated peak areas of the Mn $2p$ core-level spectra (Fig. 6) were used for calculating the Mn^{3+}/Mn^{4+} ratio. The Mn^{3+}/Mn^{4+} ratio determined by the Mn K-edge X-ray absorption near-edge structure (XANES) spectra (Fig. 2, Fig. S3, and Fig. S14) is shown for comparison.

Materials	Mn^{3+}/Mn^{4+} ratio from XPS	Mn^{3+}/Mn^{4+} ratio from XANES
CCMO(x=0.30)	1.32	0.23
CCMO(x=0.30) SPT	1.65	-
CCMO(x=0.48)	0.81	0.28

Table S6. Mn/Co and (Mn+Co)/Ca ratio of $Ca_3Co_4O_9$, $Ca_3Co_{4-x}Mn_xO_9$ (x=0.30), and $Ca_3Co_{4-x}Mn_xO_9$ (x=0.30 SPT) before and after the OER cycle stability test. The elemental ratio was determined by the SEM/EDX analysis (Fig. S2, Fig. S17, Fig. S21, and Fig. S22).

Materials	Mn/Co ratio from EDX	(Mn+Co)/Ca ratio from EDX
CCO	-	1.3
CCO after OER	-	8.1
CCMO(x=0.30)	0.15	1.3
CCMO(x=0.30) after OER	0.17	1.8
CCMO(x=0.30) SPT	0.14	1.3
CCMO(x=0.30) SPT after OER	0.13	1.3